Available online at www.eccomasproceedia.org
Eccomas Proceedia COMPDYN (2023) 4110-4124

ECCOMAS
Proceedia

COMPDYN 2023
9th ECCOMAS Thematic Conference on
Computational Methods in Structural Dynamics and Earthquake Engineering
M. Papadrakakis, M. Fragiadakis (eds.)
Athens, Greece, 12-14 June 2023

EVALUATION OF SEISMIC SITE EFFECTS IN A REAL SLOPE THROUGH 2D FE NUMERICAL ANALYSES

Annamaria di Lernia[1], Carmela Buono[2] and Gaetano Elia[1]

[1] Department of Civil, Environmental, Land, Building Engineering and Chemistry (DICATECh),
Technical University of Bari
via Orabona 4, 70125 Bari, Italy
e-mail: {annamaria.dilernia, gaetano.elia}@poliba.it

[2] Sigma Ingegneria s.r.l.
via della Libertà, 201, 90143 Palermo, Italy
carmenbuono100196@gmail.com

Abstract

The seismic site effects are the result of wave amplification processes related to the topographic irregularities, the sequence of soil layers, the morphology of the stratigraphic contacts, the dynamic properties of the soils and the input motion features. These local effects may be responsible for damages to structures and infrastructures located in different portions of the urban area, as well as they may be the trigger for landslide instability processes. In the present paper, the numerical simulations of the site effects occurring in a real natural slope have been performed through 2D finite element (FE) linear visco-elastic analyses, aiming at investigating and quantifying the influence of both the topography and the buried stratigraphy on the seismic amplification at the ground surface. The considered case study is the western slope of Chieuti, in the south of Italy, location of a deep landslide instability mechanism mainly related to static actions. After an earthquake occurred in August 2018, a worsening of the landslide-related damages affecting buildings and roads has been observed, thus requiring further investigations on the effects of the dynamic loading. Therefore, a detailed seismic geotechnical model has been developed for this case study, based on a suite of in-situ investigations, including MASW and down-hole tests. The site response analyses have been conducted with reference to three longitudinal sections and one transversal section, crossing the crest of the hillslope. The numerical results are illustrated in terms of topographic and stratigraphic amplification factors, quantifying the effect of the slope topography and the buried stratigraphy, respectively. The results show that, for this specific case study, the stratigraphic effects are predominant with respect to the topographic ones, due to the strong subsoil heterogeneity characterizing the upper portion of the slope. However, topographic effects are relevant at the crest of the hillslope, inducing further amplification of the motion.

Keywords: Seismic site response analysis, Topographic effect, Stratigraphic effect, Natural slopes, FE modelling

ISSN:2623-3347
Peer-review under responsibility of the organizing committee of COMPDYN 2023.
doi: 10.7712/120123.10705.20609

1 INTRODUCTION

It is well-known that the topographic irregularities, the sequence of soil layers, the morphology of the stratigraphic contacts and the dynamic properties of the soils, affecting the wave propagation processes, are responsible for seismic site effects [1–5]. The modification of the input motion due to the soil dynamic properties and the heterogeneity of the deposit is referred to as "stratigraphic amplification". It is related to the filtering processes of the seismic waves propagating through a medium of certain dynamic characteristics in terms of stiffness and dissipative capacity. The seismic motion may be also modified by the surface topography, giving rise to the so called "topographic amplification". These local effects may be responsible for damages to structures and infrastructures located in different portions of the urban area, as well as they may trigger or reactivate landslide instability processes [6–9].

The estimation of site effects represents a crucial issue, especially for old towns located on hilltops, characterized by urban aggregates of old masonry buildings, and for existing landslides which can be reactivated by earthquakes. In this context, an increase of the seismic demand due to topographic effects may be important in the assessment of the seismic risk of existing buildings in historical centers [10,11].

The numerical evaluation of stratigraphic effects is usually performed through one-dimensional (1D) simulations, implementing the sequence and the thickness of the soil layers and the dynamic properties of the soils [12–15]. The topographic effects are, instead, evaluated decoupling them from the stratigraphic effects, by comparing the results of two- or three-dimensional site response analyses, accounting for both stratigraphic and topographic amplification, with the output of 1D simulations, affected by the soil stratigraphy only. Numerous studies have been published in the literature on the effect of topographic amplification on the dynamic response of slopes [1,3,6,11]; most of them refers to parametric analyses of ideal case studies, assuming simplified site conditions [16–20].

In the present paper, site response analyses have been carried out through a two-dimensional (2D) FE modelling approach to investigate and quantify the influence of both the topography and the buried stratigraphy on the seismic amplification occurring at the ground surface along the western slope of Chieuti. Chieuti is a little historical hamlet in the south of Italy, location of a deep landslide instability mechanism mainly related to static actions, affecting the urban area on the crest of the hillslope [21,22]. After an earthquake of low intensity occurred on the 16th of August 2018, the landslide-related damages affecting buildings and roads have been observed to be aggravated, which has required a deeper investigation on the effects of the wave propagation processes into the slope.

The numerical simulations have been carried out with reference to a detailed subsoil model, developed on the basis of bespoke in-situ geotechnical and geophysical tests. The acceleration time history of the Montecilfone earthquake, recorded on the 16th of August 2018 at the Melanico-Santa Croce di Magliano station close to Chieuti, has been adopted in the simulations. The results have been interpreted separating the topographic effects from the stratigraphic ones, through the evaluation of appropriate amplification factors based on peak ground accelerations.

2 THE CHIEUTI CASE STUDY AND DYNAMIC CHARACTERIZATION

Chieuti (Foggia) is a small town located in the north of the Apulia region. Founded in the XV century, the old town is perched on a hilltop at 221 m a.s.l, characterized by a historic urban center with short masonry buildings and narrow alleys. The western side of the site, bounded by the Taverna stream to the north and the Fico stream valley to the west, is currently interested by an ancient landslide phenomenon, affecting the urban center since 1800 and

causing the collapse or demolition of several buildings suffering from important vertical downward displacements [21–23].

The spatial-temporal characterization of the ground displacement field has already allowed to identify the active retrogression of a progressive failure within the rear scarp of a large landslide [22]. In particular, the landsliding is characterized by multiple rotational mechanisms affecting two different bodies nested in the same toe along the Fico stream with a retrogressive evolution in time [21]. The genesis of the deep landsliding has been deemed to be related to geological processes, as demonstrated by FE hydro-mechanical simulations of the first failure corroborating the phenomenological interpretation. Indeed, the deep and retrogressive failure mechanism affecting the Chieuti area has been related to both the asymmetrical river valley erosion of the Bivento river and the surface erosion along the slope [23].

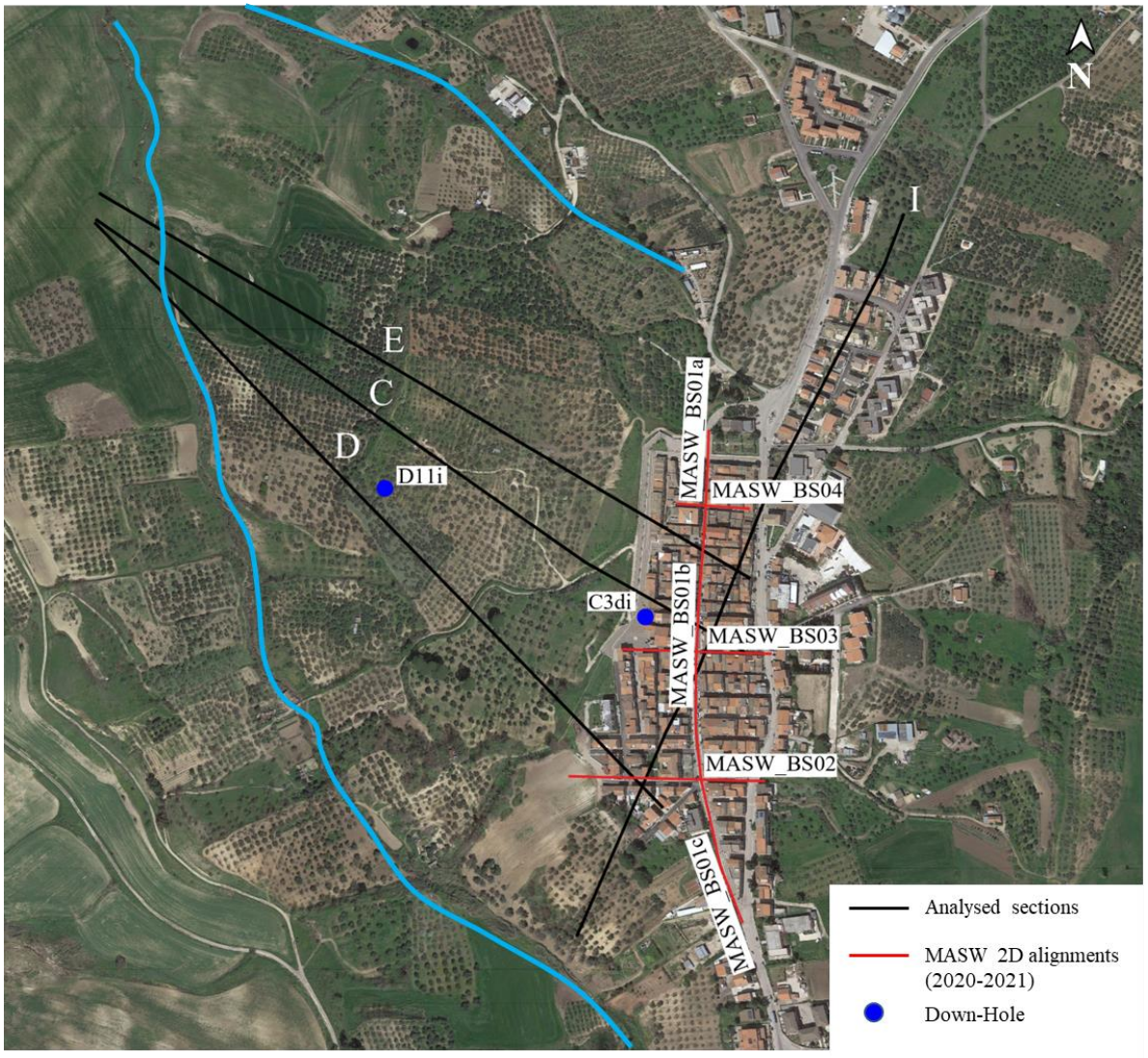

Figure 1: Orthophoto of the western slope of Chieuti and location of the in-situ geophysical tests.

From a seismic point of view, Chieuti is characterized by medium-to-high seismicity, due to the proximity to different strike-slip faults, such as the Apricena and Mattinata faults [24], which make the impact of earthquake events on slopes, buildings and infrastructures non-negligible. According to the Italian seismic hazard map [26], the Chieuti area is characterized by a PGA between 0.175g and 0.225g on the outcropping rock for a return period of 475

years. The analysis of the historical seismicity of Chieuti reveals that the site has been rarely struck by high intensity seismic events [25], among which the most important are the San Severo earthquake (30/07/1627), grade VII of the MCS, and the 2002 Molise earthquake, with 5.9 M_w.

The Chieuti hillslope is formed by a foredeep marine succession overlain by continental deposits [27,28]. The historical center is built above a top-hill thinner continental layer (*Campomarino Conglomerates* formation), made of gravel, silty, sandy and clayey intervals, deposited in an alluvial environment. The continental layer is underlain by the marine succession represented by the *Serracapriola Sands* and the *Montesecco Clay* formations. The *Serracapriola Sands* can be subdivided into two units, i.e. the lower silty-sandy unit and the upper sandy unit including local intercalation of gravel bodies, while the *Montesecco Clay* formation consists of grey marine clays with silty-sandy levels [21].

The geotechnical characterization of the slope soils has been based on the available in-situ and laboratory tests, carried out during several geotechnical campaigns, among which the last one has been conducted between December 2020 and March 2021 [21]. The analysis and the interpretation of the geotechnical characterization has allowed to identify four different materials corresponding to the sedimentary successions, i.e. Unit 1 representing the *Campomarino Conglomerates*, Unit 2a and Unit 2b associated to the upper sandy portion and the lower silty-sands portion of the *Serracapriola Sands* and Unit 3 representing the stiff marine clays belonging to the *Montesecco Clay* formation [21].

The dynamic subsoil characterization has been based on in-situ geophysical tests, including down-hole (DH) and seismic surface waves tests. Specifically, two DH tests have been carried out along the C3di (48 m deep) and D11di (70 m deep) boreholes, located within the town and in the middle of the western slope, respectively. Additionally, 2D Multi-channel Analyses of Surface Waves (MASW 2D) tests have been conducted along one longitudinal MASW_BS01 alignment and three transversal alignments, i.e. MASW_BS02, MASW_BS03 and MASW_BS04, crossing the urban center of Chieuti (Figure 1). The long MASW_BS01 test has been split along three consecutive alignments, named, from south to north, BS01c, BS01b and BS01a.

The joint interpretation of the DH and MASW 2D tests, supported by the stratigraphic information derived from the closest boreholes, has allowed to identify and to characterize the subsoil layers. The results of the DH tests are reported in Figure 2, together with the corresponding stratigraphic logs obtained from the analysis of the continuous coring performed in the C3di and C11p boreholes, the latter very close to the D11di down-hole test. Along the C3di borehole (Figure 2a), the first 18 m, where the Units 1 and 2a are encountered, are characterised by a gradual increase of velocity; the transition between the second and the third layer, i.e. Units 2a and 2b, is not significantly pronounced. This is probably due to the strong heterogeneity of the soil deposit in the upper portion of the slope, already recognised by other stratigraphic logs in the area. Along the D11di borehole (Figure 2c), the wave velocity profiles show an overall increasing trend with depth, except between 12.2 and 16.8 m of depth, where an inversion of wave velocity profile is observed at the sandy silt portion of the Unit 2b. This inversion might be associated either to the presence of inclusions of stiffer materials in the upper layer or to disturbance processes localised where the material becomes less stiff, likely due to the presence of a shear band at this depth.

Normalising the corresponding shear stiffness modulus G_0 profiles by the confining pressure p' (Figure 2b, d), it can be observed that the soils in the D11di borehole are overall stiffer than those present along the C3di vertical. With reference to the D11di stratigraphic profile, the sandy member of the Unit 2b (between 7 and 12.2 m depth) is characterised by a ratio G_0/p' significantly higher than the value evaluated along the C3di profile in the same layer

(between 18 m and 25 m). Moreover, the normalized stiffness of the silty member of Unit 2b alongside C3di (between 25 and 30 m depth) results to be higher than that obtained for the same soil layer in D11di (between 12.2 and 16.8 m depth). This indicates that, on one side, the sandy member of Unit 2b in the borehole D11di is significantly stiffer with respect to the underlaying silt member; on the other side, the silty member in D11di is particularly less stiff than the same material along the C3di profile. This circumstance might be justified by the concurrence of two effects, i.e. the strong lithological heterogeneity discovered between 7 and 12.2 m during the stratigraphic analysis and the possible presence of a shear band at a depth between 12.2 and 16.8 m, which contributes to reduce the stiffness of the material.

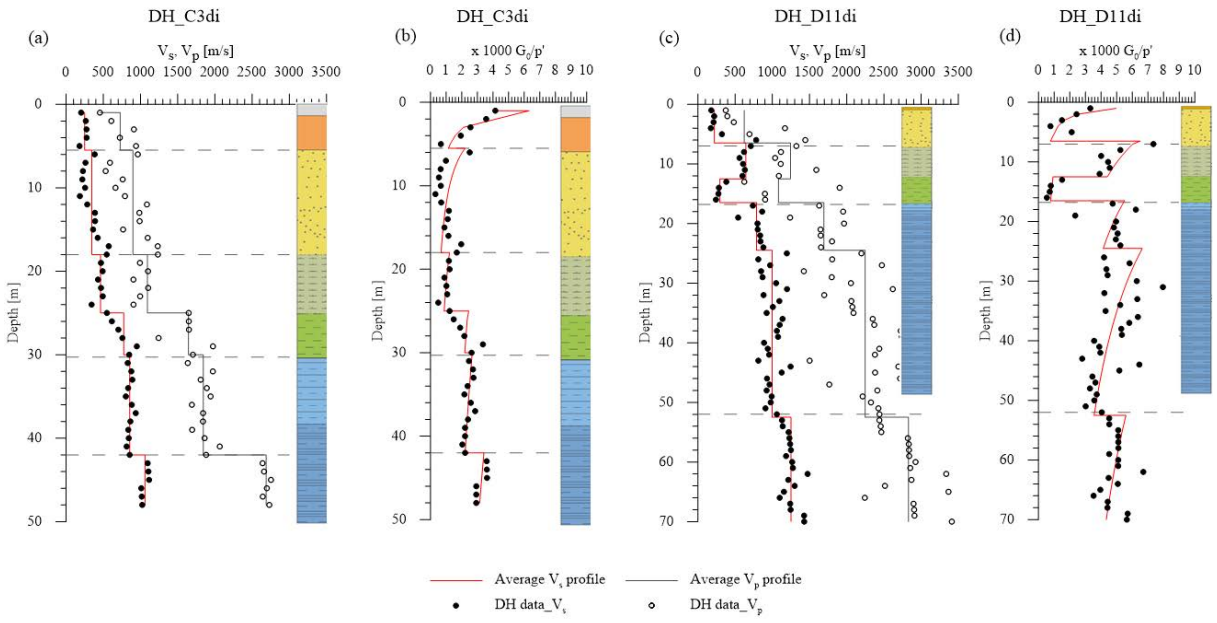

Figure 2: S- and P-wave velocity profiles and normalized shear stiffness modulus G_0/p' along the (a, b) C3di and (c, d) D11di boreholes obtained from down-hole seismic tests.

The MASW 2D tests consisted in using multiple equally-spaced receivers, placed along linear survey alignments and acquiring signals from an active impulsive source, in order to obtain 7 or 15 shear wave velocity V_s profiles along each section. The results of the MASW 2D elaboration are reported in Figure 3, together with the average V_s profile for each alignment. The detailed analysis of the V_s profiles highlights that the stiffness tends to increase with depth, starting from values of about 200 m/s, referable to the man-made material layer, and achieving values of about 800-1000 m/s for the deeper layers, coherently with the DH S-wave velocity profiles. Below the first layer, a material characterised by V_s equal to 300-400 m/s can be detected, which is ascribable to the Unit 1, followed by a stratum of 400-500 m/s of V_s, associated to the sub-unit 2a. Below this, a material with V_s of 600-700 m/s is encountered, referable to the Unit 2b, overlaying a soil layer characterised by S-wave velocity higher than 800 m/s, as expected for the deeper Unit 3 layer.

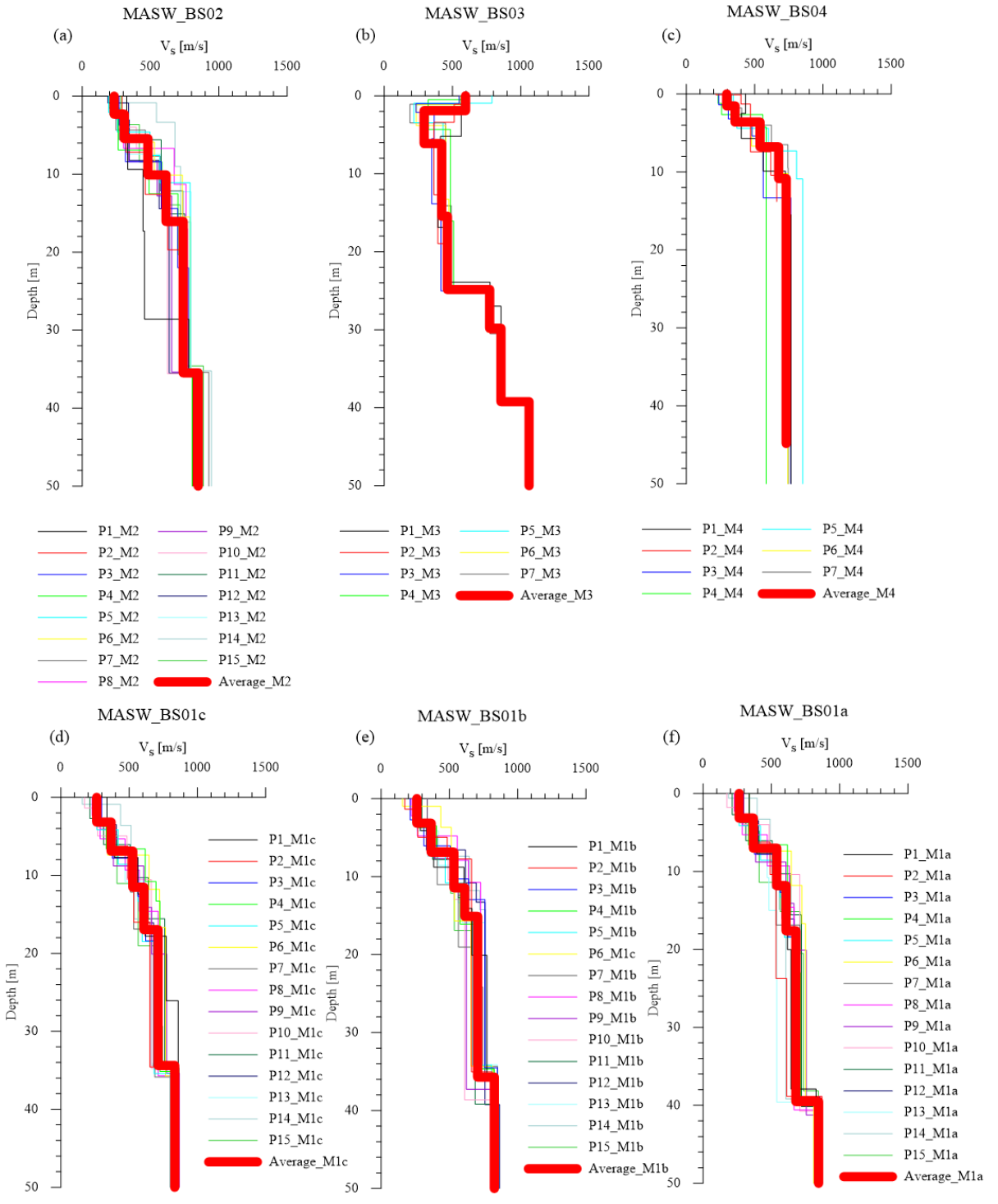

Figure 3: S-wave velocity profiles obtained from MASW2D tests along the (a) BS02; (b) BS03; (c) BS04; (d) BS01c; (e) BS01b and (f) BS01a alignments.

Using the results of these seismic in-situ investigations, the dynamic geotechnical model of the western slope of Chieuti has been constructed. Each lithological unit has been characterized by a constant value of the S-wave velocity, determined as an average value of the available measured data. The resulting model is reported in Table 1, in terms of S-wave velocity associated to each lithological unit.

Soil layer	V_s (m/s)
Man-made soil	200
Unit 1	317
Unit 2a	491
Unit 2b	627
Unit 3	871
Seismic bedrock	1250

Table 1. Dynamic geotechnical model adopted for the site response analyses.

3 NUMERICAL MODELS FOR SEISMIC RESPONSE ANALYSES

The dynamic simulations of the seismic site effects have been conducted with reference to three longitudinal sections (sections C, D and E in Figure 1) and one transversal section (section I in Figure 1) crossing the western slope of Chieuti, using the FE software PLAXIS 2D [29].

The 2D plane strain FE models are illustrated in Figure 4, only with reference to the longitudinal section C and the transversal section I, for the sake of brevity. Each investigated section is characterized by a different slope length, L_{slope}. The longitudinal sections cross the western slope of Chieuti from the highest elevation at the crest to the toe, where the impluvium is encountered. Thus, the horizontal extension of the investigated models is 771 m for section C, 806 m for section D and 745 m for section E, while the length of section I is 782 m. The average inclination of each slope model is about 9° for Section C, 8.5° for section D and 8.8° for section E. The maximum height of each longitudinal slope section, H_{right}, is 170.3 m for section C, 170 m for section D and 170 m for section E. All the geometrical models have been laterally extended by 8 times the height of the vertical sides, i.e. H_{left} and H_{right}, in order to avoid any interference of the vertical boundaries with the area of interest along the slope.

Each slope section is characterized by a sequence of Unit 1, 5 to 7 m thick, outcropping in the upper portion of the slope and overlaying the Unit 2a layer, of thickness between 15 and 20 m, in turn underlain by Unit 2b of about 8-10 m thickness. This succession overlays the Unit 3 clay soil layer. An important issue to be dealt with is the choice of the position of the top of the seismic bedrock, defined as the stratigraphic contact identifying the soil layer with V_s greater than 1200 m/s. In this case, the top of the seismic bedrock has been identified based on the DH seismic tests. Specifically, the down-hole D11di detected a material with V_s greater than 1200 m/s at a depth of 52 m b.g.l., while the seismic test identified a shear wave velocity of about 1000 m/s at a depth of 40 m under the urban center along the C3di. Thus, the subsoil under the town is most likely characterized by V_s greater than 1000 m/s at depth greater than 40 m. Therefore, the top of the seismic bedrock has been defined parallel to the sloping ground surface at a depth of 50 m b.g.l. The shear wave velocity values implemented in the FE models are summarized in Table 1 for each soil layer.

The soil behavior has been simulated with a linear visco-elastic model, characterized by a constant unit weight of 19 kN/m^3, Poisson's ratio equal to 0.33, at-rest earth pressure coefficient K_0 equal to 0.5. The damping ratio has been implemented through the Rayleigh formulation [30], where the control frequencies f_m and f_n have been selected equal to 1 Hz and 12 Hz with a target damping D^* of 5%, ensuring that an average damping ratio of 3%, representative of the dissipative capacity of the involved soils in the 0.001% - 0.01% strain range, is implemented in the model.

The 2D soil domain of each slope model has been discretized with 15-node triangular elements, distributed such that a greater refinement is obtained approaching the ground surface. Specifically, Section C has been discretized with 18154 elements, Section D consists of

19571 elements, Section E is composed of 22114 elements, while Section I is characterized by 19770 elements. On the top surface of each model, the nodes have a maximum distance equal to the predominant wavelength of the Rayleigh waves ($\lambda_R \cong 0.94 \cdot V_s/f_{max}$), to capture the frequency content of the travelling surface waves. In the vertical direction, the node distance has been set equal to one eighth of the wavelength ($\lambda_S \cong V_s/f_{max}$) associated to the maximum frequency of the seismic excitation (assumed equal to 20 Hz), in order to capture the frequency content of the seismic excitation [31].

During the static stage, performed with the K_0-procedure, standard boundary conditions have been applied to the slope models, consisting in imposing total fixities to the nodes at the bottom of the mesh and horizontal fixities to the nodes at the lateral sides of the models. After the initial static stage, the dynamic simulations have been conducted by adopting the *free field* boundary conditions at the vertical sides of the model, simulating the free field conditions, and the *compliant base* boundary [32] at the bottom of the mesh, simulating the dissipation of the waves into the deep soil layers with minimum reflection at the bottom boundary. In this case, the input motion is applied to the main domain in terms of normal and shear stress time histories. Since only the upward propagating waves should be considered in the signal applied at the *compliant base*, only half of the input motion is prescribed at the base of the FE model.

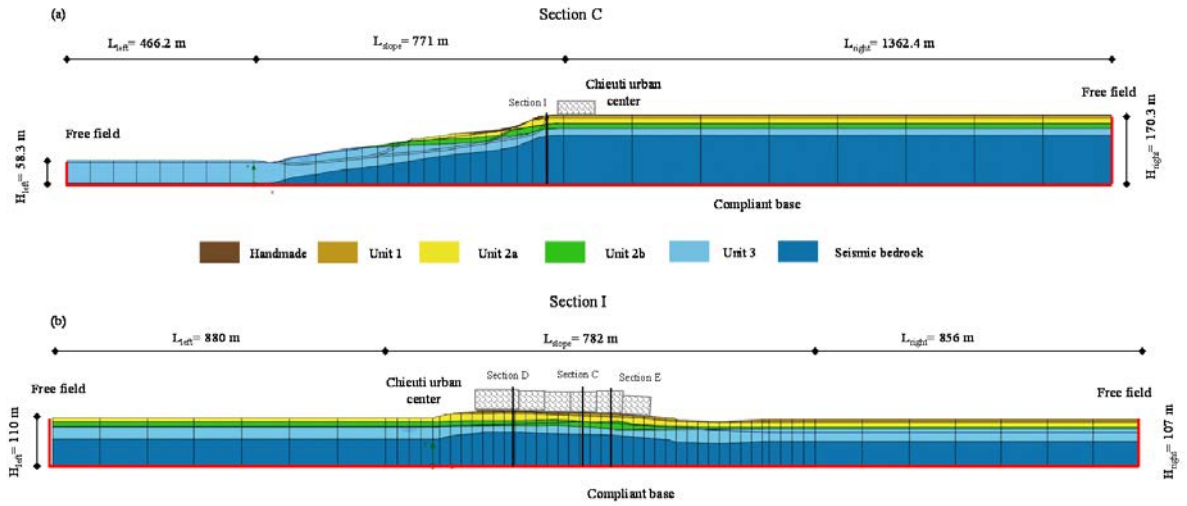

Figure 4: 2D FE models of the longitudinal section C and the transversal section I.

The seismic motion adopted in the dynamic simulations refers to the earthquake occurred at Montecilfone (Campobasso, Molise) on the 16th of August 2018, characterised by M_w equal to 5.2 and epicentral depth of 20 km. The acceleration time history (Figure 5a), recorded at the Melanico-Santa Croce di Magliano station (MELA station), is characterized by a duration of 50 s, a peak ground acceleration (PGA) of 0.022g and a high frequency content covering a range up to 20 Hz (Figure 5b). The predominant period T_p of the input motion has been identified to be equal to almost 0.1 s (Figure 5c).

All the dynamic analyses have been carried out under the assumption of fully undrained conditions. The Generalized Newmark method has been employed as time integration scheme during the dynamic stage, with Newmark parameters α_N and β_N equal to 0.25 and 0.5, respectively, which implies that no numerical damping is introduced in the FE simulations. A time step of 0.01 s has been adopted, largely fulfilling the required constrain suggested by Bathe [31].

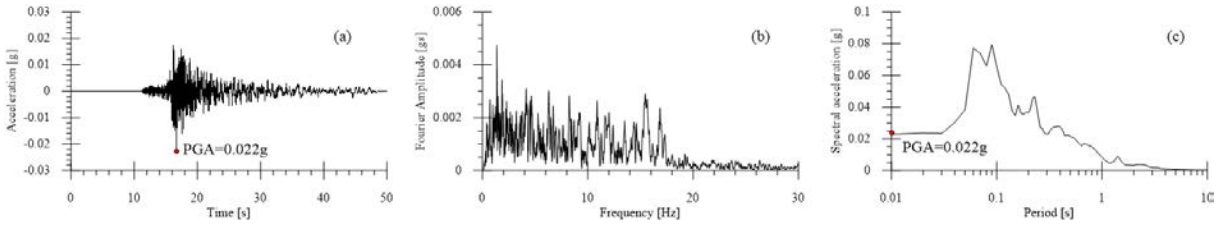

Figure 5: Seismic event occurred on the 16th of August 2018 recorded at the Melanico-Santa Croce di Magliano station: (a) acceleration time history, (b) Fourier spectrum and (c) response spectrum.

4 EVALUATION OF THE TOPOGRAPHIC AND STRATIGRAPHIC EFFECTS

The computed 2D site response is presented here in terms of total amplification factor *AF*, defined as the ratio between the absolute value of the peak ground acceleration $a_{\max,s}$ recorded at a given observation point on the ground surface of each 2D slope model and the maximum acceleration of the input motion, $a_{\max,i}$, i.e. 0.022g:

$$AF = \frac{a_{\max,s}(2D)}{a_{\max,i}} \tag{1}$$

The distribution of the amplification factors *AF* at the ground surface for each slope section (Figure 6) highlights that the seismic input motion is significantly amplified at the crest of the slope and in its middle portion at the distance between 300 m and 640 m for section C (Figure 6a), between 300 m and 710 m for section D (Figure 6b) and between 300 m and 610 m for section E (Figure 6c). Conversely, a typical valley effect is observed at the topographic impluvium, as expected, where the propagating input motion suffers from a de-amplification at the ground surface. A similar and unexpected de-amplification of the input motion is also detected in the upper portion of the slope at the distance between 640 m and 700 m for section C (Figure 6a), between 710 m and 750 m for section D (Figure 6b) and between 610 m and 660 m for section E (Figure 6c). The maximum amplification factors, attaining values between 2.1 and 1.7, are detected at the crest of the longitudinal sections. The minimum values of *AF* for each longitudinal section are between 0.8-0.9, highlighting a de-amplification of the input motion both at the toe and in the upper portion of the slope.

With the aim of separating the topographic from the stratigraphic amplification effects and quantifying how much the total amplification is due to either the stratigraphy of the buried subsoil or the topographic profile of the slope, stratigraphic and topographic amplification factors have been computed. To this purpose, additional numerical simulations have been carried out with reference to 1D models, accounting for the soil layer amplification only, built with reference to the stratigraphic conditions of each 2D longitudinal section.

Specifically, the stratigraphic amplification factor AF_S is defined as the ratio of the peak ground acceleration at the top of the 1D model and the maximum acceleration of the input motion, $a_{\max,i}$, i.e. 0.022g:

$$AF_S = \frac{a_{\max,s}(1D)}{a_{\max,i}} \tag{2}$$

The topographic amplification factor AF_T is, instead, defined as the ratio between 2D and 1D peak ground accelerations:

$$AF_T = \frac{a_{\max,s}(2D)}{a_{\max,s}(1D)} \tag{3}$$

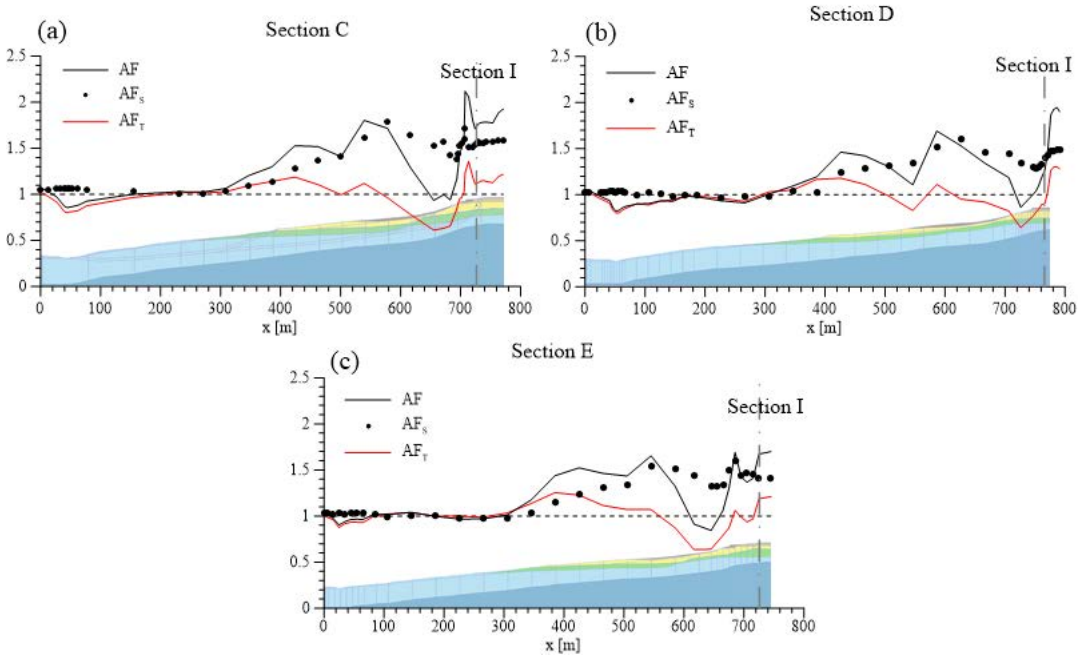

Figure 6: Distribution of the total amplification *AF*, topographic amplification AF_T and stratigraphic amplification AF_S factors for (a) section C, (b) section D and (c) section E.

The distributions of the amplification factors along each slope section are illustrated in Figure 6. For all the examined longitudinal sections, the AF_T distribution shows fluctuations around the unit value. Moreover, the AF_T factors are always lower than the AF_S values, highlighting the more pronounced influence of the soil stratigraphy with respect to the slope topography on the seismic amplification processes. However, the effects due to the topography should not be neglected. Indeed, while the AF_S achieves maximum values between 1.6 and 1.8 in the middle portion of the slope, the topographic amplification factor AF_T reaches maximum values between 1.2 and 1.4 at the crest of the slope. Therefore, the high values of the total amplification factors observed at the crest of the slope are related not only to the subsoil heterogeneous stratigraphy, but also to the focalization of the seismic waves due to the topographic profile. The de-amplification of the seismic motion at the impluvium is clearly due to the presence of the valley, as confirmed by the AF_T distribution reducing to values lower than 1, where AF_S attains values around 1.

As previously observed, the computed 2D response shows an unexpected seismic de-amplification in the upper portion of the slope, i.e. between 600 m and 750 m depending on the considered longitudinal section, which is clearly not an effect of the soil stratigraphy as revealed by the AF_S distribution. In fact, this could be due to either the topography of the slope or to the morphology of the buried subsoil, non-horizontally layered in these parts of the slope.

To quantify the influence of the subsoil heterogeneity and the morphology of the stratigraphic contacts of the soil layers on the ground amplification, further 2D numerical simulations have been performed implementing an equivalent homogeneous soil layer resting on the seismic bedrock, whose dynamic properties are representative of the average behavior of the examined subsoil. Thus, an equivalent shear wave velocity value has been defined according to Eq. 4:

$$V_{S,eq} = \frac{H}{\sum_{i=1}^{n} \frac{h_i}{V_{s,i}}} \tag{4}$$

where H is the thickness of the homogeneous soil layer resting on the seismic bedrock, i.e. 50 m in the present case study, h_i and $V_{s,i}$ are the thickness and the shear wave velocity of the soil layer, respectively, constituting the soil stratigraphy along each longitudinal section. It should be noted that, since the subsoil stratigraphy is not horizontally layered and variable thickness of soil units are detected along each slope section, different values of the equivalent shear wave velocity for each slope section can be expected, as reported in Table 2.

Section	$V_{s.eq}$ (m/s)
C	491
D	471
E	478
I	480

Table 2. Values of the equivalent shear wave velocity adopted for the homogeneous slope models.

The heterogeneity amplification factor AF_H may well be defined as the ratio between the peak ground acceleration of the 2D heterogenous model, $a_{\max,s}$ (2D), and the peak ground acceleration of the 2D equivalent homogeneous model, $a_{\max,s,eq}$ (2D):

$$AF_H = \frac{a_{\max,s}(2D)}{a_{\max,s,eq}(2D)} \tag{5}$$

The distributions of the total amplification factor, computed for both the heterogenous (AF) and the homogeneous (AF_{eq}) slope models, are illustrated in Figure 7 for each slope section, together with the heterogeneity AF_H amplification factor. The 2D homogeneous models of the longitudinal sections (Figure 7a-c) are characterized by total amplification factors AF_{eq} attaining values close to 1, especially between 300 m and 650 m (depending on the considered section), clearly indicating a small amplification if the slope is assumed homogeneous. Furthermore, the valley and the canyon effects are emphasized in correspondence of the impluvium and at the crest of the slope, respectively, where AF_{eq} reaches values between 0.7 and 0.8 at the toe of the slope and between 1.1 and 1.2 at the crest. Indeed, the AF_H profile clearly shows the predominant influence of the subsoil heterogeneity in amplifying the seismic motion on the ground surface between 300 m and about 650 m. Conversely, in the upper portion of the slope between 600 m and 750 m, the de-amplification of the seismic motion is related more to the slope topography than to the buried subsoil features. Indeed, in these portions the heterogeneity amplification factors AF_H along each longitudinal section are characterized by values of about 0.7-0.8. The reason for this response lies in the morphology of the slope profile, characterized by a local variation in the surface inclination, forming a sort of valley. In particular, the sloping surface changes its inclination from 8° to 21° along section C, from 9° to 20° along section D and from 10° to 16° along section E where the minimum AF_H is attained. At the crest of the slope, a combination of stratigraphic and topographic effects might be detected, as confirmed by the AF_H profiles along the longitudinal sections.

With reference to the transversal section I (Figure 7d), the AF_{eq} profile shows a flat pattern characterized by values between 0.8 and 1. Conversely, the AF_H profile attains the minimum value of 1.5 in the southern area (left side of the 2D model), where the Unit 2a outcrops, and the maximum value of 2.4 in the middle portion of the section, between the intersection with

sections C and D, where the Unit 1 is outcropping. Thus, the heterogeneity characterizing the subsoil at the crest of the slope might be deemed to be responsible for the seismic amplification at the ground surface, although the topographic irregularities are also contributing to the wave propagation process, as revealed by the comparison between AF and AF_S, reported in the figure at the intersection with the longitudinal sections only.

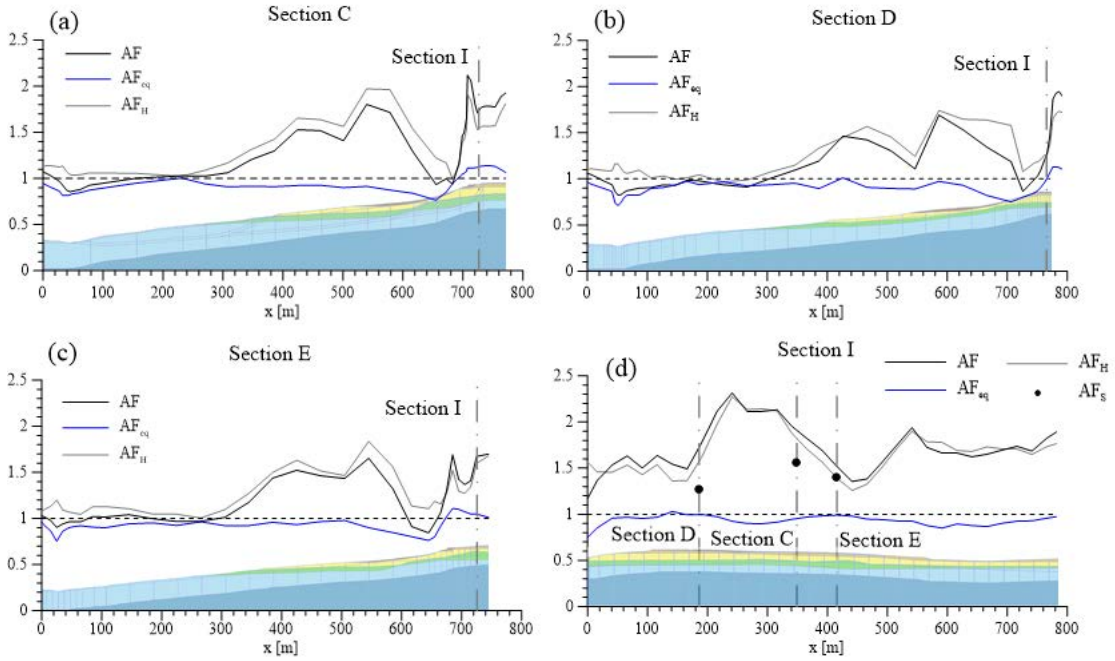

Figure 7: Distribution of the total amplification factors evaluated for the heterogeneous (AF) and equivalent homogeneous (AF_{eq}) slope models and the heterogeneity amplification factor AF_H for (a) section C, (b) section D, (c) section E and (d) section I.

5 CONCLUSIONS

The present paper is aimed at evaluating and identifying the seismic site effects affecting a real natural slope, the western slope of Chieuti in the south of Italy, using a 2D FE numerical approach. The topographic effects have been decoupled from the stratigraphic effects through the separate evaluation of the topographic and stratigraphic amplification factors.

The numerical simulations revealed that the stratigraphic effects are predominant for most of the slope, while the topographic effects play a significant role in its upper portion, where the focalization of the seismic waves occurs. Indeed, the strong heterogeneity characterizing the subsoil of Chieuti is mostly responsible for the seismic ground surface amplification affecting the urban area. Although the topographic amplification factors are not significantly high for the specific case study, the topographic effects can also play an important role in the wave propagation process, as the input motion is amplified by 1.2-1.4 at the crest, where the buildings are located. Thus, neglecting these topographic effects, as suggested by the Italian Building code [33] for slope angles lower than 15°, could be detrimental for a proper assessment of the seismic vulnerability of the structures.

The analyses of the seismic site response of different slope sections allowed to identify the area of the hillslope mostly affected by the seismic amplification phenomena. Indeed, the slope portion characterized by high amplification factors is the crest of the slope, as a result of the combination of the topographic irregularities and the heterogeneity of the buried subsoil.

Moreover, the highest amplification factors are detected in the southern part of the slope crest between sections C and D.

ACKNOWLEDGEMENTS

The research has been supported by the PON-AIM project (AIM1871082) and the PON-MITIGO project (ARS01_00964). The third author is grateful for the financial support received by the project "National Centre for HPC, Big Data and Quantum Computing – Spoke 5: Environment and Natural Disasters" (CN_00000013) funded by the National Recovery and Resilience Plan (NRRP), M4_C2_1.4 – NextGenerationEU.

REFERENCES

[1] D. Assimaki, G. Gazetas, E. Kausel, Effects of local soil conditions on the topographic aggravation of seismic motion: parametric investigation and recorded field evidence from the 1999 Athens earthquake. *Bulletin of the Seismological Society of America*, **95**(3), 1059–1089, 2005.

[2] L. Geli, P.Y. Bard, B. Jullien, The effect of topography on earthquake ground motion: A review and new results. *Bulletin of the Seismological Society of America*, **78**(1), 42–63, 1988

[3] G.A. Athanasopoulos, P.C. Pelekis, E.A. Leonidou, Effects of surface topography on seismic ground response in the Egion (Greece) 15 June 1995 earthquake. *Soil Dynamics and Earthquake Engineering*, **18**(2), 135–149, 1999.

[4] G. Biondi, M. Maugeri, Seismic response analysis of the Monte Po hill (Catania). In *Seismic prevention of damage. A case study in a Mediterranean City*, Southampton, UK, 2005.

[5] Y. Fukushima, K. Irikura, T. Uetake, H. Matsumoto, Characteristics of Observed Peak Amplitude for Strong Ground Motion from the 1995 Hyogoken Nanbu (Kobe) Earthquake. *Bulletin of the Seismological Society of America*, **90**(3), 545–565, 2000.

[6] G. Gazetas, P.V. Kallou, P.N. Psarropoulos, Topography and Soil Effects in the MS 5.9 Parnitha (Athens) Earthquake: The Case of Adámes. *Natural Hazards*, **27**, 133–169, 2002.

[7] K.O. Cetin, A.G. Papadimitriou, S. Altun, P. Pelekis, B. Unutmaz, E. Rovithis, et al, The role of site effects on elevated seismic demands and corollary structural damage during the October 30, 2020, M7.0 Samos Island (Aegean Sea) Earthquake. *Bulletin of Earthquake Engineering*, **20**(14), 7763–7792, 2022.

[8] Y. Yin, F. Wang, P. Sun, Landslide hazards triggered by the 2008 Wenchuan earthquake, Sichuan, China. *Landslides*, **6**, 139–152, 2009.

[9] E. Bertrand, A.M. Duval, J. Régnier, R.M. Azzara, F. Bergamaschi, P. Bordoni, et al, Site effects of the Roio basin, L'Aquila. *Bulletin of Earthquake Engineering*, **9**, 809–823, 2011.

[10] F. Sabetta, G. Fiorentino, F. Bocchi, M. Sinibaldi, G. Falcone, A. Mendicelli, Influence of local site effects on seismic risk maps and ranking of Italian municipalities. *Bulletin of Earthquake Engineering*, 1–28, 2023.

[11] A. Pagliaroli, G. Lanzo, B. D'Elia, Numerical Evaluation of Topographic Effects at the Nicastro Ridge in Southern Italy. *Journal of Earthquake Engineering*, **15**(3), 404–432, 2011.

[12] J. Régnier, L. Bonilla, P. Bard, E. Bertrand, F. Hollender, H. Kawase, et al, International Benchmark on Numerical Simulations for 1D, Nonlinear Site Response (PRENOLIN): Verification Phase Based on Canonical Cases. *Bulletin of the Seismological Society of America*, **106**(5), 2112-2135, 2016.

[13] A. di Lernia, A. Amorosi, D. Boldini, A multi-directional numerical approach for the seismic ground response and dynamic soil-structure interaction analyses. *7ICEGE. VII International Conference on Earthquake Geotechnical Engineering,* Rome, Italy, 2019.

[14] G. Falcone, D. Boldini, A. Amorosi, Site response analysis of an urban area: A multi-dimensional and non-linear approach. *Soil Dynamics and Earthquake Engineering*, **109**, 33–45, 2018.

[15] J. Régnier, L. Bonilla, P. Bard, E. Bertrand, F. Hollender, H. Kawase, et al, PRENOLIN: International Benchmark on 1D Nonlinear Site‐Response Analysis—Validation Phase Exercise. *Bulletin of the Seismological Society of America*, **108**(2), 876‐900, 2018.

[16] G.D. Bouckovalas, A.G. Papadimitriou. Numerical evaluation of slope topography effects on seismic ground motion. *Soil Dynamics and Earthquake Engineering*, **25**(7–10), 547–558, 2005.

[17] A.G. Papadimitriou, S.A. Paraskevopoulos, A.N. Lamprakopoulos, Aggravation of spectral acceleration along 2D symmetrical trapezoidal valleys. *16th European Conference on Earthquake Engineering*, Thessaloniki, Greece, 2018.

[18] A.G. Papadimitriou. An engineering perspective on topography and valley effects on seismic ground motion. *7ICEGE. VII International Conference on Earthquake Geotechnical Engineering*, Rome, Italy, 2019.

[19] S. Rizzitano, E. Cascone, G. Biondi, Coupling of topographic and stratigraphic effects on seismic response of slopes through 2D linear and equivalent linear analyses. *Soil Dynamics and Earthquake Engineering*, **67**, 66–84, 2014.

[20] Z. Zhang, J.A. Fleurisson, F. Pellet, The effects of slope topography on acceleration amplification and interaction between slope topography and seismic input motion. *Soil Dynamics and Earthquake Engineering*, **113**, 420–431, 2018.

[21] F. Santaloia, A. di Lernia, S. Guglielmi, L. Pisano, A. Sonnessa, M. Stragapede, et al, Phenomenological analysis and monitoring of a slow-moving paleo-landslide affecting an urban area. *Engineering Geology*, in prep.

[22] A. Sonnessa, A. di Lernia, D.O. Nitti, R. Nutricato, E. Tarantino, F. Cotecchia, Integration of Multi-sensor MTInSAR and ground-based geomatic data for the analysis of non-linear dis-placements affecting the urban area of Chieuti, Italy. *International Journal of Applied Earth Observation and Geoinformation*, **117**, 103194, 2023.

[23] V. Tagarelli, F. Santaloia, G. Elia, F. Cotecchia, Numerical modelling of the geological processes responsible for mid-Pleistocene landslide inception: an insight into possible factors for the current landslide activity. *10th European Conference on Numerical Methods in Geotechnical Engineering*, London, UK, 2023.

[24] E. Patacca, P. Scandone, The 1627 Gargano earthquake (Southern Italy): Identification and characterization of the causative fault. *Journal of Seismology*, **8**(2), 259–273, 2004

[25] M. Locati, R. Camassi, A. Rovida, E. Ercolani, F. Bernardini, V. Castelli, et al, DBMI15, the 2015 version of the Italian Macroseismic Database. *Istituto Nazionale Di Geofisica e Vulcanologia*, 2016.

[26] M. Stucchi, C. Meletti, V. Montaldo, H. Crowley, G.M. Calvi, E. Boschi, Seismic Hazard Assessment (2003-2009) for the Italian Building Code. *Bulletin of Seismological Society of America*, **101**(4), 1885–1911, 2011.

[27] A. Amorosi, V. Bracone, V. Di Donato, C.M. Rosskopf, P.P.C. Aucelli, The Plio–Pleistocene succession between Trigno and Fortore rivers (Molise and Apulia Apennines): stratigraphy and facies characteristics. *GeoActa*, **8**, 1–12, 2009.

[28] V. Bracone, A. Amorosi, P.P.C. Aucelli, C.M. Rosskopf, F. Scarciglia, V. Di Donato, et al, The Pleistocene tectono-sedimentary evolution of the Apenninic foreland basin between Trigno and Fortore rivers (Southern Italy) through a sequence-stratigraphic perspective. *Basin Research*, **24**(2), 213–233, 2012.

[29] PLAXIS 2D CE V20, *PLAXIS CONNECT Edition V20. Reference manual*, 2020.

[30] J. Rayleigh, *The theory of sound*. New York, Dover, 1945.

[31] K.J. Bathe, *Finite Element Procedures*. 2nd ed. Upper Saddle River, Prentice Hall, 1996.

[32] W.B. Joyner, A.T.F. Chen, Calculation of nonlinear ground response in earthquake. *Bulletin of Seismological Society of America*, **65**(5), 1315–1336, 1975.

[33] CS.LL.PP. Norme tecniche per le costruzioni. *Gazzetta Ufficiale della Repubblica Italiana*, 2018.